JOURNAL OF VIROLOGY, Sept. 2011, p. 9414–9424 Vol. 85, No. 18
0022-538X/11/$12.00 doi:10.1128/JVI.00281-11

Autophagosome Formation during Varicella-Zoster Virus Infection following Endoplasmic Reticulum Stress and the Unfolded Protein Response▽†‡

John E. Carpenter,[1] Wallen Jackson,[1] Luca Benetti,[2] and Charles Grose[1]*

Children's Hospital, University of Iowa, Iowa City, Iowa,[1] and Vaccine Manufacturing Sciences and Commercialization, Merck Manufacturing Division, West Point, Pennsylvania[2]

Received 8 February 2011/Accepted 17 March 2011

Autophagy is a recently recognized component of the life cycle of varicella-zoster virus (VZV). We have documented abundant autophagosome formation in skin vesicles (final site of virion assembly) from randomly selected cases of varicella and zoster. The fact that autophagy was an early event in the VZV replication cycle was documented by finding infected vesicle cells with the VZV IE62 protein confined to the nucleus. Next, we pursued studies in VZV-infected cultured cells to define whether autophagy was preceded by endoplasmic reticulum (ER) stress and the unfolded protein response (UPR). First, we demonstrated that autophagosome formation in infected cells closely resembled that seen after treatment of cells with tunicamycin, a potent initiator of ER stress. Second, we demonstrated a marked expansion of ER size in both VZV-infected cells and cells transfected with the predominant VZV glycoprotein complex gE/gI. An enlarged ER is critical evidence of ER stress, which in turn is relieved by the UPR. To this end, we documented the UPR by detecting the alternatively spliced form of the XBP1 protein as well as CHOP (C/EBP homologous protein), both transcriptional activators of other UPR genes in an ER stress-dependent manner. Because VZV does not encode inhibitors of autophagy, the above results suggested that autophagy was a common event in VZV-infected cells and that it was provoked at least in part by ER stress secondary to overly abundant VZV glycoprotein biosynthesis, which led to UPR activation in an attempt to maintain cellular homeostasis.

Varicella-zoster virus (VZV) is a human pathogen that causes chicken pox (varicella) and shingles (zoster) (55). Zoster is the disease associated with reactivation of latent VZV in the elderly. The virus exists as a spherical particle approximately 200 nm in diameter, including a 125-kb DNA genome enclosed in an icosahedral capsid which is itself surrounded by an amorphous shell of proteins called the tegument and an outer lipid envelope containing viral glycoproteins (9). The most prominent viral glycoprotein is called gE and is part of the gE/gI complex (20, 22). Within a few days after infection, viral replication leads to the assembly of nascent viral particles in the head and neck region. A viremia ensues within T lymphocytes, after which viral particles exit the capillaries and replicate within the epidermis to cause the characteristic vesicular rash (28). The skin vesicle is considered to be the final site of assembly and envelopment of the mature VZ virion (52). Relatively little is known about the innate immune response within the cutaneous microenvironment (2).

How a cell responds to viral infection and in turn how the virus attempts to moderate that response have been a topic of renewed research. One such response of the host cell is to increase macroautophagy (29). Macroautophagy is a catabolic process by which whole or parts of organelles are sequestrated into double-membraned autophagosomes in the cytoplasm and then degraded when the autophagosomes fuse with lysosomes (48, 56). Autophagy frees amino acids and other metabolites for use in other cellular processes. Viral peptides are generated by the degradation process and become available for presentation on the cell surface via major histocompatibility complex (MHC) (11, 18). Thus, autophagy is thought to play a role in both innate and adaptive immunity (12). Recent reviews summarize the range of interactions between viruses and the autophagic process (19, 31, 45). Some RNA viruses, for example, hepatitis C virus, have coopted the autophagy mechanism to produce viral particles (14, 15). On the other hand, a complex DNA virus closely related to VZV, namely, herpes simplex virus 1 (HSV-1), actively inhibits the formation of autophagosomes via its ICP34.5 protein (34). VZV lacks an ICP34.5-homologous protein (10). Therefore, it was of interest when we showed that autophagy is a prominent feature in cultured cells infected with VZV, as demonstrated by immunoblotting for the LC3B marker protein as well as the autophagy adaptor p62/SQSTM1 (47). Further, we observed numerous cytoplasmic organelles with distinctive double outer membranes characteristic of autophagosomes within electron microscopic images of the same VZV-infected cells.

Here we extend earlier observations by showing that autophagosomes are a prominent and easily detectable feature in both primary VZV infection and reactivated VZV infection in humans. Further, we show that VZV infection of cultured cells induces endoplasmic reticulum (ER) stress and the unfolded protein response (UPR) to that stress. The UPR is a series of signal pathways by which a stressed cell attempts to recover homeostasis by suspending protein translation, expanding the

* Corresponding author. Mailing address: University of Iowa Hospital/2501 JCP, 200 Hawkins Drive, Iowa City, IA 52242. Phone: (319) 356-2270. Fax: (319) 356-4855. E-mail: charles-grose@uiowa.edu.

† Supplemental material for this article may be found at http://jvi.asm.org/.

▽ Published ahead of print on 13 July 2011.

‡ The authors have paid a fee to allow immediate free access to this work.

TABLE 1. Primary antibodies used in this study

Antibody	Type	Antigen	Source (reference)
3B3	Murine monoclonal	VZV gE	Our laboratory (23)
6B5	Murine monoclonal	VZV gI	Our laboratory (20)
5C6	Murine monoclonal	VZV IE62	Our laboratory (43)
258	Murine monoclonal	VZV gH	Our laboratory (48)
R19	Rabbit polyclonal	VZV gC	Our laboratory (48)
GP gE	Guinea pig polyclonal	VZV gE	Our laboratory (8)
L7543	Rabbit polyclonal	LC3B	Sigma
sc-7160	Rabbit polyclonal	XPB1	Santa Cruz Biotechnology
sc-793	Rabbit polyclonal	GADD153/CHOP	Santa Cruz Biotechnology
1620	Murine monoclonal	Keratin	Chemicon
OKT3	Murine monoclonal	CD3	Ebioscience
sc-7219	Rabbit polyclonal	CD4	Santa Cruz Biotechnology
18-0119	Murine monoclonal	CD8	Invitrogen
333802	Murine monoclonal	CD68	BioLegend

ER, facilitating degradation processes via ER-associated degradation (ERAD), and increasing autophagy (42). The Alwine laboratory has shown that cytomegalovirus (CMV), a betaherpesvirus, selectively induces ER stress and uses components of the UPR (particularly BiP) to form a viral assembly compartment proximal to the ER (5, 24). If the stressed cell fails to recover homeostasis, the UPR will initiate apoptosis.

In the VZV system, we hypothesized that overly abundant viral glycoprotein biosynthesis leads to ER stress, with increased autophagy being the result of the subsequent UPR to that stress. We tested our hypothesis by comparing autophagosome formation following VZV infection with that induced by tunicamycin, a chemical that blocks glycoprotein biosynthesis in the ER and thereby initiates ER stress. We also probed for both the alternatively spliced form of the X box protein 1 (XBP1) and the CCAAT/enhancer-binding protein homologous protein (CHOP), both transcriptional activators of the UPR in response to ER stress and therefore excellent markers for ER stress (43). Our cumulative results suggest a role for ER stress and autophagy in VZV pathogenesis during both primary and reactivated infections. This role appears to be remarkably different from that proposed for autophagy during HSV infection (29, 30).

MATERIALS AND METHODS

Viruses and cells. VZV-32 is a low-passage-number laboratory strain; its genome has been completely sequenced and falls within the European clade of VZV genotypes (37). MRC-5 fibroblast cells and HeLa cells were grown on 12-mm round or 22-mm square coverslips in minimal essential medium with Earle's salts (E-MEM) supplemented with 10% fetal bovine serum (FBS). When cells were nearly confluent, they were inoculated with VZV-infected cells at a ratio of one infected cell to eight uninfected cells by previously described methods (21). Preparations of cells from vesicle samples from patients with chicken pox and zoster were collected and stored in our laboratory, as part of an earlier study described by Weigle and Grose (54).

Primary and secondary antibodies. Primary antibodies used in this study are listed by type and source in Table 1. We thank C. Morita (University of Iowa) for murine monoclonal antibody (MAb) OKT3 to human CD3 and J. Fairley (University of Iowa) for murine MAb 1620 to human keratin. The secondary antibodies included Alexa 488, 546, and 633 fluoroprobes conjugated to goat anti-rabbit IgG or goat anti-guinea pig or goat anti-mouse IgG $F(ab')_2$ fragment (Invitrogen).

Construction of plasmids. VZV genes were amplified by PCR from DNA isolated from cultured cells infected with the laboratory strain VZV-32. The primer sequences for VZV gene inserts were the following: ORF68 (gE), 5′-GGGGAGCTCCCATGGGGACAGTTAATAAACC-3′ (NcogE, sense); ORF68 (gE), 5′-CCCGGGTCTTATCTATATACACCGTGTA-3′ (Sma1gE, antisense); ORF67 (gI), 5′-CGGCTCACAGAGCTGCTCTTCGGTGTAG-3′ (scp1, sense); ORF67 (gI), 5′-TAATCCTTCCCCTCATATCACAACGCGT-3′ (scp2, antisense); ORF37 (gH), 5′-CGGTGATATTGTAGCGCAAGTAACAGC-3′ (sp10, sense); ORF37 (gH), 5′-CCCAAAGGTAGTGTGTATTATTCGCG-3′ (sp11, antisense); ORF60 (gL), 5′-CAAGCGCCATGGCATCACATAAAT-3′ (p1, sense); ORF60 (gL), 5′-AAACACTAGTCCATGTGCATGTCCCGC-3′ (p2, antisense). The PCR-amplified DNA was ligated into the mammalian expression plasmid pTargeT containing the CMV immediate-early (IE) promoter (Promega). The resulting plasmids were amplified in component DH5α *Escherichia coli* (Invitrogen) and isolated with the plasmid midikit (Qiagen). The PCMV_IE62 plasmid was kindly provided to us by W. T. Ruyechan (University of Buffalo) (36). The plasmids were transfected into HeLa cells using Fugene 6 (Roche) transfection reagent (25) at 5 μl/ml and plasmid DNA at a concentration of 0.5 μg/ml. After 6 h of incubation, the culture medium was replaced with plasmid-free medium.

Imaging protocols. Samples of infected and uninfected cells were prepared for confocal microscopy by methods described previously (7). Briefly, the samples were fixed with paraformaldehyde and permeabilized with 0.05% Triton X-100 in phosphate-buffered saline (T-PBS) and then blocked in 5% nonfat milk with 2.5% normal goat serum for 2 h at room temperature (RT). The primary antibody (1:2,000) was added for 2 h at RT and overnight at 4°C. After washing (3 times for 5 min each), the samples were incubated with the secondary antibody (1:1,250) and the Hoechst 33342 double-stranded DNA (dsDNA) stain (1:500) for 2 h at RT before washing (3 times for 5 min each) and mounting on slides for viewing. Following preparation, the samples were viewed on Zeiss 510 and 710 confocal fluorescence microscopes (16).

Samples were processed for scanning electron microscopy by methods described previously (7). Briefly, following initial fixation with paraformaldehyde and antibody labeling steps, the sample was further fixed with 4% glutaraldehyde in PBS and then stained with 1% OsO_4 in double-distilled water (ddH_2O), followed by dehydration in a graded series of ethanol-water mixtures from 25% ethanol to 100% ethanol and then 100% hexamethylene disilane (HMDS). Finally, the sample was air dried and mounted on aluminum stubs. Images of the mounted samples were viewed with a Hitachi S-4800 scanning electron microscope.

Tunicamycin protocol. Conditions for treatment of cultured cells with tunicamycin (2.5 μg/ml; Calbiochem; catalog no. 654380) have been described in earlier papers in which we were investigating VZV glycoprotein biosynthesis (8, 32). For experiments in uninfected cells, tunicamycin (2.5 μg/ml) was added 24 h after subculturing and the monolayer was fixed after another 24 h.

Dicarbocyanine dye localization. $DiOC_6$ (3-3-dihexyloxacarbocyanine iodide) was obtained in powder form from Molecular Probes (D-273) and dissolved (0.7 mg/ml) in ethanol (41). An aliquot of the $DiOC_6$ stock (2.8 μl/ml yielded a final concentration of $DiOC_6$ of 2 μg/ml) was added to warm cell culture medium; this medium was applied to live cells for 30 min and then rinsed twice with phosphate-buffered saline (PBS) and processed for fluorescence microscopy as described above.

SDS-PAGE and immunoblotting. Methods for SDS-PAGE and immunoblotting have been previously described by this laboratory (8). Electrophoresis was performed in precast 4 to 15% gradient acrylamide gels (Ready Gel; Bio-Rad). Proteins in the gel were then transferred to a polyvinylidene difluoride (PVDF) membrane (Immobilon-P; Millipore). The membrane subsequently was blocked with 5% nonfat milk containing 2.5% normal goat serum (Sigma) in T-PBS for 2 h and then incubated in the primary antibody (1:500 in T-PBS) for 2 h at RT and overnight at 4°C. Following washing (3 times for 5 min each), the membrane was incubated in goat anti-rabbit or anti-mouse secondary horseradish peroxidase (HRP) antibody (A10547 and F21453, respectively; Invitrogen) for 2 h at RT and then washed 5 times for 5 min each. Thereafter, the membrane was incubated in chemiluminescent solution (Super Signal West Pico solution, P34080; Thermo Scientific) for 5 min at RT. Finally, the membrane was patted dry and exposed to autoradiography film.

RESULTS

Enumeration of the cellular constituents within a vesicle. We characterized the type and relative population of vesicle cells by antibody labeling and fluorescent imaging. Specifically,

TABLE 2. Characterization of cell population from a zoster vesicle[a]

Antigen	No. of images	No. of cells	% positive	SD (%)
Keratin	8	987	77.9	7.7
CD3	9	185	22.4	7.9
CD4	12	197	13.1	12.5
CD8	10	1,632	11.8	4.7
CD68	20	1,148	6.8	4.9

[a] Cells were collected from a zoster vesicle onto several glass slides as previously described (54). Subsequently, individual slides were antibody labeled with each of the fluorescent probes and a nuclear stain. Approximately 10 images at 200× were examined on a Zeiss 710 confocal fluorescent microscope. Total cells in each image were counted based on the nuclear stain, and then those specifically labeled by antibody were enumerated to arrive at a percentage that was positive for a particular probe.

sequentially collected samples from human zoster vesicles from the same patient were labeled with antibodies to keratin as well as T-cell and macrophage markers: CD3, CD4, CD8, and CD68. The immunostained samples were then viewed at 200×, and approximately 10 images were taken of each sample. Total cells in an image were counted on the basis of the nuclear staining; antibody-positive cells were distinguished on the basis of the specific probe. Some caution was required because a few cells, particularly keratinocytes, autofluoresced when exposed to laser light less than 500 nm in wavelength. Generally, we found that approximately 75% of the cells were keratinocytes while 25% were T cells or macrophages (Table 2). Among the lymphocyte population, approximately half were $CD4^+$ and the other half were $CD8^+$. Our vesicle samples usually were collected during the early days of rash; it is possible that samples collected later would contain a different ratio of lymphocytes and macrophages.

Identification of infected keratinocytes within a vesicle. Using the same samples, we found that virtually all keratinocytes were infected while only a small number of lymphocytes were infected (Fig. 1). For example, a typical image showed a wide scattering of cells with several small clumps of keratinocytes (Fig. 1A). Within this set of images, a small number of cells did not stain for keratin (Fig. 1A, white solid arrows) and were likely T cells. Most but not all of the keratinocytes stained positively for VZV gC, indicating that they were infected (Fig. 1B). Although some keratinocytes (Fig. 1, white dotted arrows) showed little VZV gC reactivity and likely were uninfected or early in the infection cycle, the majority of keratinocytes within a large clump of cells stained positively for VZV gC (Fig. 1C and D). On the other hand, a small number of T cells around the clump (several marked by white arrows) exhibited no VZV gC labeling. We postulate that this clump of the cells represented the base of a vesicle and that the T cells were either attached to the inner wall or found nearby in the vesicle fluid.

To confirm the presence of viral particles, one of the vesicle samples was processed for viewing with a scanning electron microscope. Within a clump of cells, we observed a cluster of viral particles (marked by white arrows) above what appeared to be a capillary opening (Fig. 1E and F). This image confirmed prior observations that viral particles in skin vesicles are prototypic in appearance (6).

Surveillance for autophagosomes in cells from human varicella vesicles. Autophagosomes are distinguished by the presence of the distinctive LC3B-II membrane protein, which is detected by specific antibody immunolabeling (26, 49). Although we had previously observed autophagosomes in a zoster vesicle, neither we nor others have examined a varicella vesicle, to determine if autophagy is a component of the cellular response to primary VZV infection as well as VZV reactivation. To this end, we examined cells in two different samples obtained from human varicella vesicles (Fig. 2). The cells were immunolabeled with rabbit antibody (RAb) against LC3B and mouse MAb against VZV gE. We have previously

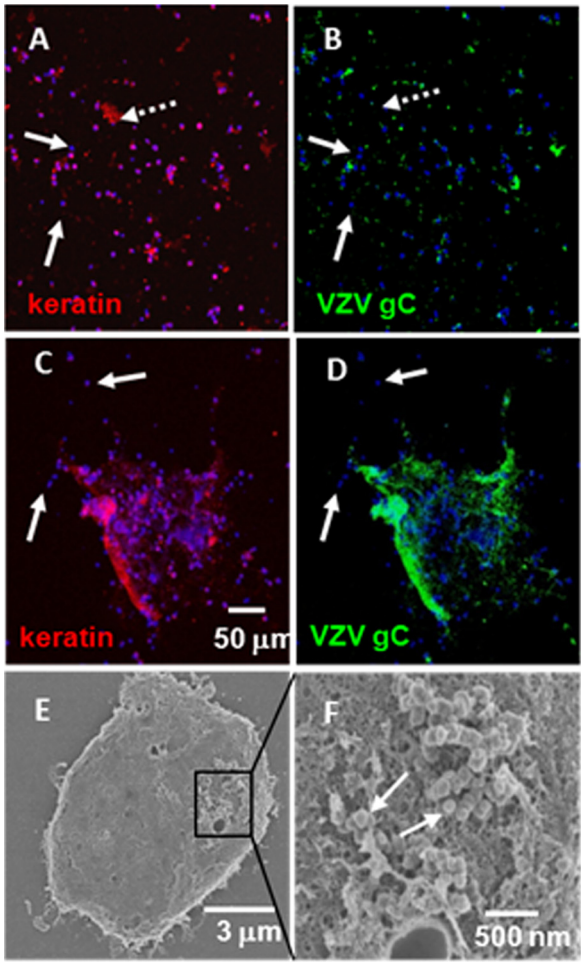

FIG. 1. Vesicle samples consisted mostly of infected keratinocytes and uninfected lymphocytes. Cells from zoster and varicella vesicles were collected onto glass slides and later labeled with fluorescent probes to keratin and VZV gC in addition to a DNA stain (Hoechst 33342). Later, several of the samples were processed for imaging with a scanning electron microscope. (A and B) Typical cellular distribution within a sample, where most cells were positive for keratin and were infected. A few cells (solid white arrows) were lymphocytes and were not infected. There was one notable keratin mass (dotted white arrow) that was not infected. (C and D) A cellular mass where the majority of the cells were keratinocytes (C) and were infected (D); this cluster was surrounded by a smaller number of cells (white arrows) that were likely uninfected lymphocytes. (E and F) Scanning electron microscopic images of an infected cellular mass that included keratinocytes (E) with a cluster of VZV viral particles (white arrows) emerging above a capillary opening (F). Note that all VZV-specific antibody reagents are described in Table 1.

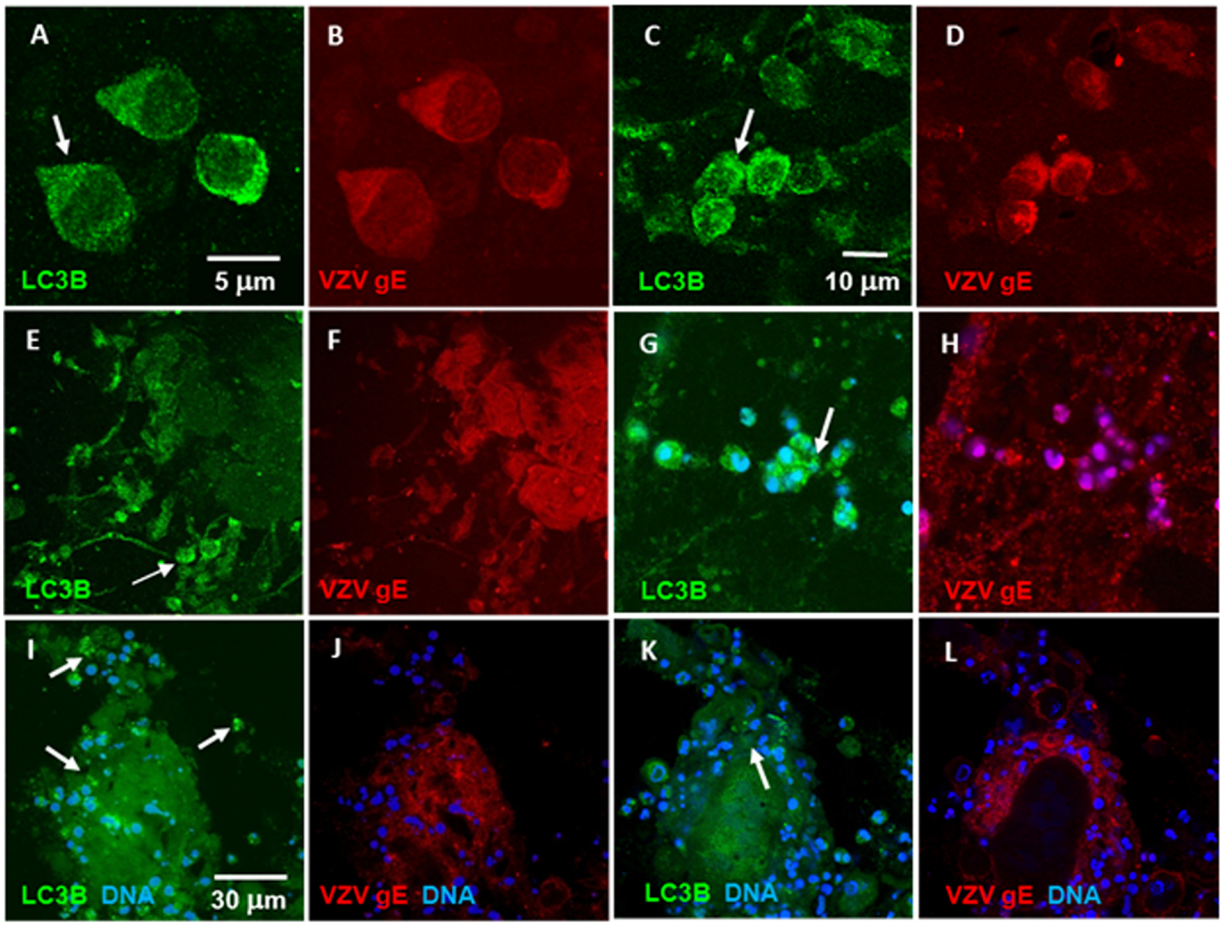

FIG. 2. Autophagosomes were observed in infected keratinocytes from zoster and varicella vesicles. Cells from varicella and zoster vesicles were collected as described and subsequently antibody labeled with fluorescent probes to LC3B and VZV gE plus a DNA stain. LC3B puncta were indicative of LC3B-II in the outer wall of autophagosomes. Examples are marked by white arrows. (A to D) Two instances from different vesicles of several infected keratinocytes that exhibited numerous LC3B-positive fluorescent puncta. (E and F) Large tissue mass in which several cells exhibited punctate LC3B staining patterns similar to the cells in panel A. (G and H) Small cluster of infected cells exhibited extensive LC3B puncta. (I to L) Two Z-stack slices of infected keratinocytes showed a diffuse LC3B staining pattern in the interior of the tissue while cells near the periphery exhibited LC3B-positive puncta. Similarly to panels in Fig. 1, there were several uninfected cells that also lacked LC3B puncta; these cells were likely lymphocytes. See also Fig. S1 in the supplemental material.

shown by traditional fluorescence microscopy that virtually all infected cells collected from humans with varicella contain VZV gE protein, the most abundant VZV protein (54). Upon further examination by confocal fluorescence microscopy, we quickly documented that the majority of keratinocytes from the floor of a vesicle that stained positively for VZV antigens (red) also reacted with the LC3B antibody (green) in the cytoplasm, as shown in representative panels A to L of Fig. 2. Three cells were selected for higher-magnification images (Fig. 2A and B); the cells were both infected (as indicated by the red staining in Fig. 2B) and contained a large number of autophagosomes in the cytoplasm (green puncta in Fig. 2A). When larger clumps of infected cells (Fig. 2E to H and I to L) were observed, autophagosomes were often visible on the periphery of the clump (white arrows), a pattern suggesting that, in VZV-infected skin vesicle cells, autophagy may be detected in recently infected cells as well as in cells at later stages of viral replication. Additional images of VZV-infected cells from a vesicle are shown in Fig. S1 in the supplemental material.

Within the above samples, we counted 130 cells within 23 confocal images. Of these, 95 were VZV gE-positive infected cells (73%). This percentage of infected cells was similar to the overall number of keratinocytes in the vesicle samples; this result confirmed that virtually all of the collected keratinocytes were infected while few of the T cells were VZV positive. Among the infected cells, 69 (72%) also contained punctate autophagosomes.

Detection of autophagosomes during immediate-early (IE) kinetic phase of VZV replication. To extend the above observations and further assess the hypothesis that autophagy is upregulated early in infection, we immunostained additional varicella vesicle samples with antibodies to LC3B and VZV IE62. VZV IE62 is the major viral transcriptional regulator that localizes to the nucleus early in the infection (first 8 h), thus becoming an excellent marker for the immediate-early to early kinetic phases of infection (17). Later in the replication cycle, IE62 relocates into the cytoplasm. A few cells in a vesicle sample were found to be newly infected, based on the presence

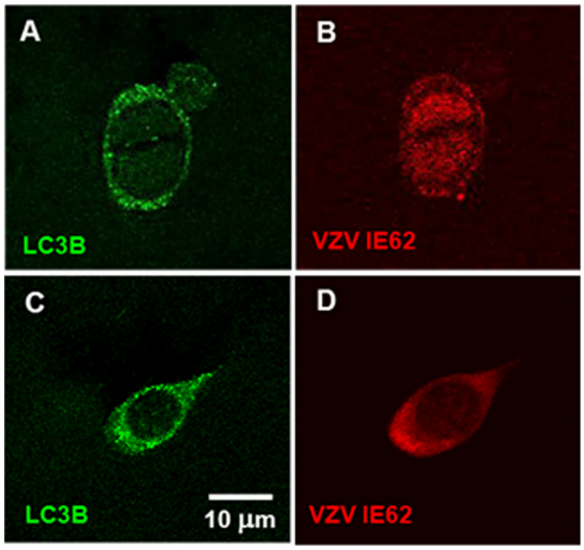

FIG. 3. Autophagosomes were observed in infected keratinocytes expressing nuclear VZV IE62 protein. Cells from varicella vesicles were collected as described and antibody labeled with fluorescent probes to LC3B and VZV IE62. (A and B) A single keratinocyte with a bifid nucleus exhibited LC3B puncta characteristic of LC3B-II in autophagosomes, while VZV IE62 immunoreactivity was detected in the nuclei. (C and D) A more typical infected keratinocyte showed both punctate LC3B staining and IE62 immunoreactivity in the cytoplasm.

of IE62 in the nucleus. In these infected keratinocytes, punctate LC3B-positive autophagosomes were detected in the cytoplasm (Fig. 3A and B). Most of the cells, obviously in a later stage of infection, immunostained positively for both LC3B and VZV IE62 in the cytoplasm (Fig. 3C and D). The above results confirmed and extended our prior data in infected cultured cells, which showed that viral VZV replication was not required for induction of autophagy, and therefore, that induction of autophagy did not require the late kinetic phase of infection. Furthermore, these cumulative data in human vesicle cells substantiated the idea that autophagy in cultured infected cells was a good representation of autophagy in human VZV disease.

Effects of tunicamycin on autophagy in uninfected and VZV-infected cells. We previously described a prominent punctate LC3B staining pattern in VZV-infected MRC-5 cells compared with a diffuse pattern in uninfected cells (47). Here we show that the punctate pattern of LC3B immunoreactivity in VZV-infected MRC-5 cells was virtually identical to the punctate pattern seen in uninfected MRC-5 cells treated with tunicamycin (Fig. 4A to E). In all, we observed 19 of 311 (6.1% ± 2.2%) mock-treated cells which exhibited moderate LC3B puncta (e.g., Fig. 4C) while 91 of 284 (32.0% + 8.4%) tunicamycin-treated cells exhibited extensive LC3B puncta (e.g., Fig. 4A and D; see also Fig. S2 in the supplemental material). Tunicamycin is a mixture of antibiotics that inhibits virtually all N-linked glycosylation in the ER, thus inducing a robust and rapid ER stress response (33, 51). We subsequently postulated that the addition of tunicamycin to VZV-infected cells would allow us to determine whether additional autophagy would be stimulated by both events within an infected cell. The fact that tunicamycin treatment did not further enhance formation of autophagosomes over VZV infection alone suggested that VZV infection induced a maximal ER stress response (Fig. 4F). IE62 was found primarily in the nucleus (white arrows in Fig. 4F), confirming the prior observation that VZV-induced autophagy occurred early even in the presence of tunicamycin. As an incidental finding, we also observed that some cells in Fig. 4F exhibited fragmented nuclei—a hallmark of apoptosis (red arrows) (23). The combined effects of stress of VZV infection combined with tunicamycin treatment likely tipped the UPR into inducing apoptosis even in cells at early stages of viral replication, as indicated by the nuclear localization of IE62.

Expanded ER as a marker of the unfolded protein response to ER stress during VZV infection. As noted previously in an authoritative review, one hallmark of the unfolded protein response to ER stress is an expanded ER (13, 43). We examined VZV-infected MRC-5 fibroblasts by transmission electron microscopy (TEM) and observed grossly extended ER folds in infected cells (black arrows, Fig. 5A and B). Of interest, the increased folds of the ER had the characteristics of smooth ER. The TEM images of an enlarged ER during VZV infection also closely matched those of butyrate-treated cells published previously by the Kaufman laboratory (13).

To quantify the increase in the size of the ER due to VZV infection, we measured the relative size of the ER in VZV-infected MRC-5 cells by staining the cells with $DiOC_6$, a polar dye that preferentially localizes to polarized membranes, such as those found in mitochondria and the ER (41, 50). A series of confocal fluorescent images at 630× were then taken of both uninfected and VZV-infected MRC-5 cells. Within each image, ellipses were drawn around the ER/nucleus complex (Fig. 5C) and then around each nucleus. After the major and minor axes of the ellipses were measured, we computed an area for the ER/nucleus complex and the nuclei alone. The ER area was obtained by subtracting the area of the nuclei from that of the ER/nucleus complex. The ratio of the ER area to the nuclear area was then plotted by the number of occurrences of a given ratio (Fig. 5, graph). Using this resultant ratio has the advantage of minimizing any effect of choice of focal plane in the image on the areas being measured. The distribution of values for the ratio of ER to nucleus area in the uninfected cells was normal with an average of 0.28 ± 0.12, while the distribution of the same ratio in infected cells was not normal and varied broadly from 0.5 to almost 7.0. The largest ratios were found mostly in multinucleated syncytia, while the lowest ratios likely were found in newly infected single cells. VZV-infected MRC-5 cells form only modest syncytia involving fewer than 10 nuclei (e.g., Fig. 4E). The above observation suggested that the ER in VZV-infected cells can be up to 10 times larger in area than that in uninfected cells—a clear sign of ER stress.

Autophagosome formation after transient expression of VZV glycoproteins. During viral replication, many viral gene products, including viral glycoproteins, are expressed to very high levels, thus potentially creating the conditions necessary to induce ER stress and subsequent autophagy (20, 22). To test the hypothesis that expression of VZV glycoproteins in VZV-infected cells during active replication is sufficient to cause ER stress and autophagy, we transiently expressed four major

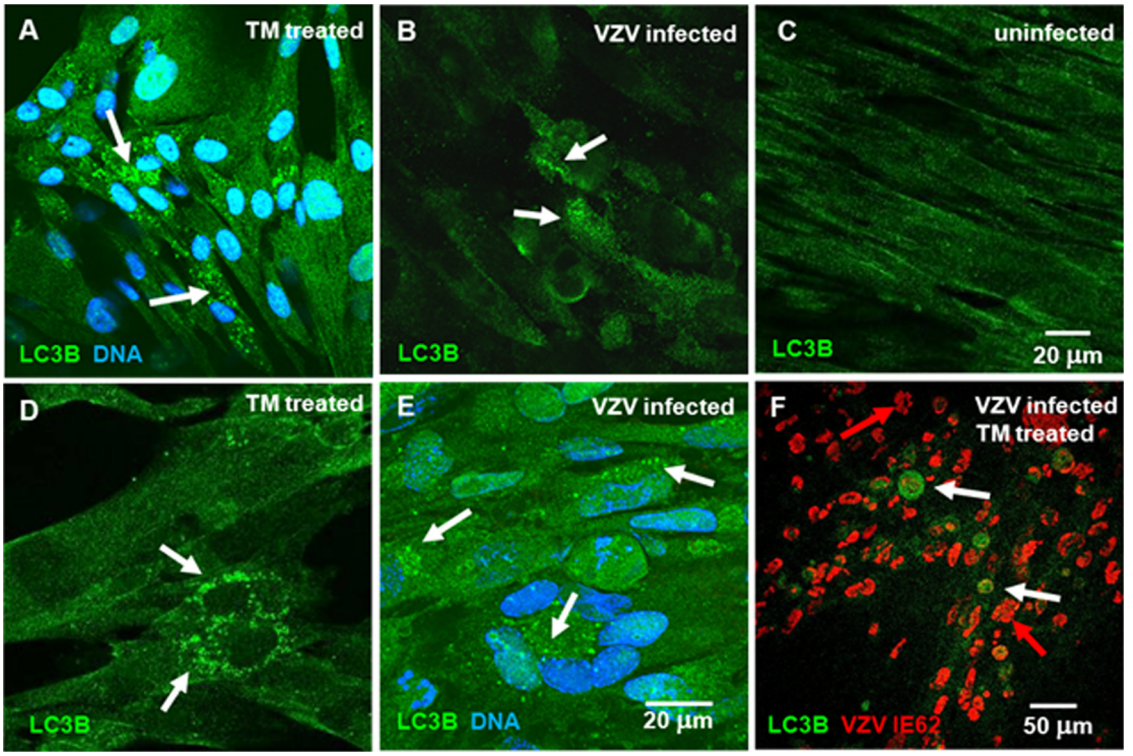

FIG. 4. Tunicamycin-induced autophagosomes in uninfected cells were similar to those induced by VZV infection in cultured cells. One monolayer of MRC-5 cells was grown to confluence and treated with tunicamycin for 24 h before fixation. A second culture was inoculated with VZV-infected cells and incubated for 72 h before fixation. A third culture was inoculated with VZV-infected cells, treated with tunicamycin at 6 hpi, and then fixed at 24 hpi. The samples were then immunolabeled with anti-LC3B antibody and imaged with a confocal microscope. Some samples were also labeled with a nuclear DNA stain and a VZV-specific antibody (Table 1). (A and D) Tunicamycin (TM)-treated uninfected cells demonstrated punctate staining (white arrows) characteristic of autophagosomes. (B and E) VZV-infected cells showed increased LC3B punctate immunoreactivity indicative of autophagosomes near the perinuclear area of infected cells, similar to LC3B punctate staining seen in tunicamycin-treated uninfected cells. (C) Uninfected MRC-5 cells exhibited relatively uniform diffuse LC3B staining without individual puncta. (F) Tunicamycin treatment of VZV-infected cells induced similar levels of punctate LC3B staining early in the infectious cycle, as indicated by the large number of cells with VZV IE62 protein (red) still in the nucleus. Tunicamycin is a known inducer of ER stress, because the compound blocks all N-linked glycoprotein biosynthesis in the ER. A number of the cells exhibited fragmented nuclei typical of apoptotic cells (red arrows) in the latter panel. Also see Fig. S2 in the supplemental material.

VZV structural glycoproteins—gE (ORF68), gI (ORF67), gH (ORF37), and gL (ORF60)—in HeLa cells, under the control of the CMV early promoter in PTargeT plasmids. We then examined the cells for increased LC3B puncta by confocal fluorescence microscopy. Of interest, we discovered that autophagosome formation was highly sensitive to the transfection conditions, particularly the length of incubation after transfection. Cells expressing VZV gE (Fig. 6A1 to A4), VZV gI (Fig. 6B1 to B4), or VZV gE and VZV gI together (Fig. 6C1 to C4) or VZV gH and VZV gL (Fig. 6D1 to D4) together displayed large LC3B-positve puncta proximal to the ER early (8 to 24 h posttransfection) in the incubation period. Later in the incubation period (>24 h posttransfection), many of the cells that expressed VZV glycoproteins showed evidence of apoptosis (data not shown). Overall, we collected 70 images from 6 sets of transfection cultures that differed in incubation times (6 to 48 h) and antibody probes. Altogether, we counted 729 cells within these images, of which 225 were expressing VZV gE and/or VZV gI or VZV gH and gL for a transfection rate of 31%. The overall percentage of transfected cells that displayed these puncta was 19% (42 of 225), suggesting that increased autophagy associated with transient VZV glycoprotein expression was both early and temporally short lived.

Further, we note that two cells expressing VZV gE/gI appeared to have recently divided from a common cell (Fig. 6C1 to C4). Other investigators found that K562 (human myeloblastoid leukemia) cells and HeLa cells in the G_2 or M cell cycle phase were more likely to be transfected when using lipoplex (e.g., formed by a cationic lipid such as Lipofectamine 2000) or polyplex (e.g., formed by a cationic amino polymer such as Fugene 6) transfection compounds (4, 53). They interpreted this finding as suggesting that the DNA plasmid is only slowly imported into the nucleus via a nuclear pore but moves rapidly into the nucleus when the nuclear membrane is dissolved during mitosis.

Control experiments were carried out using Fugene 6 alone or a commercial plasmid expressing enhanced green fluorescent protein (EGFP), under the control of the CMV promoter (Clontech). After counting over 500 cells in each culture, we found a basal rate of LC3B-positive punctum formation of 2% ± 2% in each experiment (data not shown). This basal rate may be accounted for by the observation that autophagy is

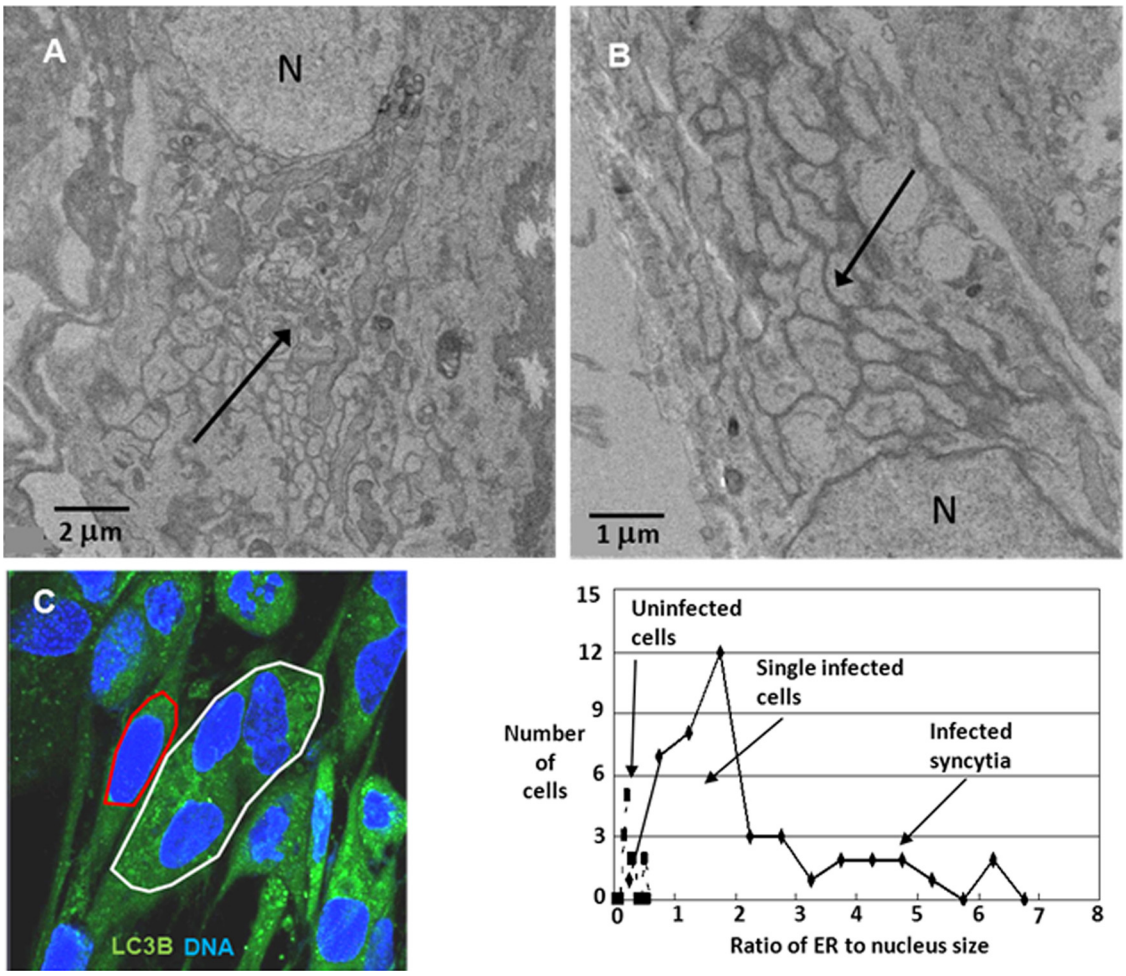

FIG. 5. VZV infection resulted in an enlarged ER, indicative of ER stress. MRC-5 cells were grown to confluence, inoculated with VZV-infected cells, and then incubated for another 72 h. One set of samples was processed for viewing in a transmission electron microscope, and a second set was processed for fluorescence microscopy. (A and B) Enlarged ER folds and multiple chambers (black arrows) were visualized in infected cells. N, nucleus. (C) Another set of samples was then stained with 2 mM $DiOC_6$, a lipophilic polar dye, for 30 min as described in Materials and Methods. The cells were then incubated with a nuclear stain and imaged at 630× with a Zeiss 710 confocal fluorescence microscope. Using ImageJ software, ellipses were drawn around the ER/nuclear complex of single cells (e.g., red ellipse) or multinuclear syncytia (e.g., white ellipse) in order to determine the area of ER and the nuclei in that focal plane. The ratio of ER to nuclear area was then calculated and plotted. The graph showed that the ER size in uninfected cells was one-third of the nuclear size, whereas in infected cells that ratio was 5 to 10 times larger, particularly for multinucleated syncytia.

required for midbody ring disposal during cell division (38). Above, we reported that increased LC3B-positive puncta were observed early in the VZV replication process in vesicle cells as indicated by the presence of VZV IE62 in the nucleus of the infected cell. To test whether transient transfection of IE62 alone using a plasmid construct under the CMV promoter was sufficient to induce increased autophagy, we counted 344 cells of which 88 were transfected and observed a rate of IE62-expressing cells exhibiting LC3B-positive puncta of 2% ± 3% (representative images are included in Fig. S3 in the supplemental material). Such a rate was similar to the rate obtained with Fugene alone or when using a GFP-expressing plasmid and considerably lower than the rate observed for cells transfected with VZV glycoproteins. Of note, many of the cells transfected with IE62 were observed to progress to cell death via apoptosis or autophagy-associated cell death much sooner (24 h) than those transfected with VZV glycoproteins (data not shown). Thus, the above experiments supported our hypothesis that constitutive expression of a VZV glycoprotein, which would occur in the ER, was sufficient to increase autophagy in transfected cells.

ER expansion after transient expression of VZV glycoproteins. To expand our hypothesis about an expanded ER as a marker of ER stress and autophagy, we quantified the size of the ER in HeLa cells transfected with plasmids expressing VZV gE, using the same methodology as described for VZV-infected cells (Fig. 7). In a representative image showing cells stained with $DiOC_6$, one cell was expressing VZV gE (Fig. 7A); the ER was noticeably larger and brighter than that in other cells. Subsequently, the ER and ER/nuclear areas were measured in 71 cells in 5 images, 20 of which were expressing VZV gE and plotted in a manner similar to the graph in Fig. 5. Of interest, we observed that nontransfected HeLa cells (expressing no VZV glycoprotein) exhibited a higher ER-to-nuclear area ratio (1.0) than did MRC-5 cells (0.3). Perhaps

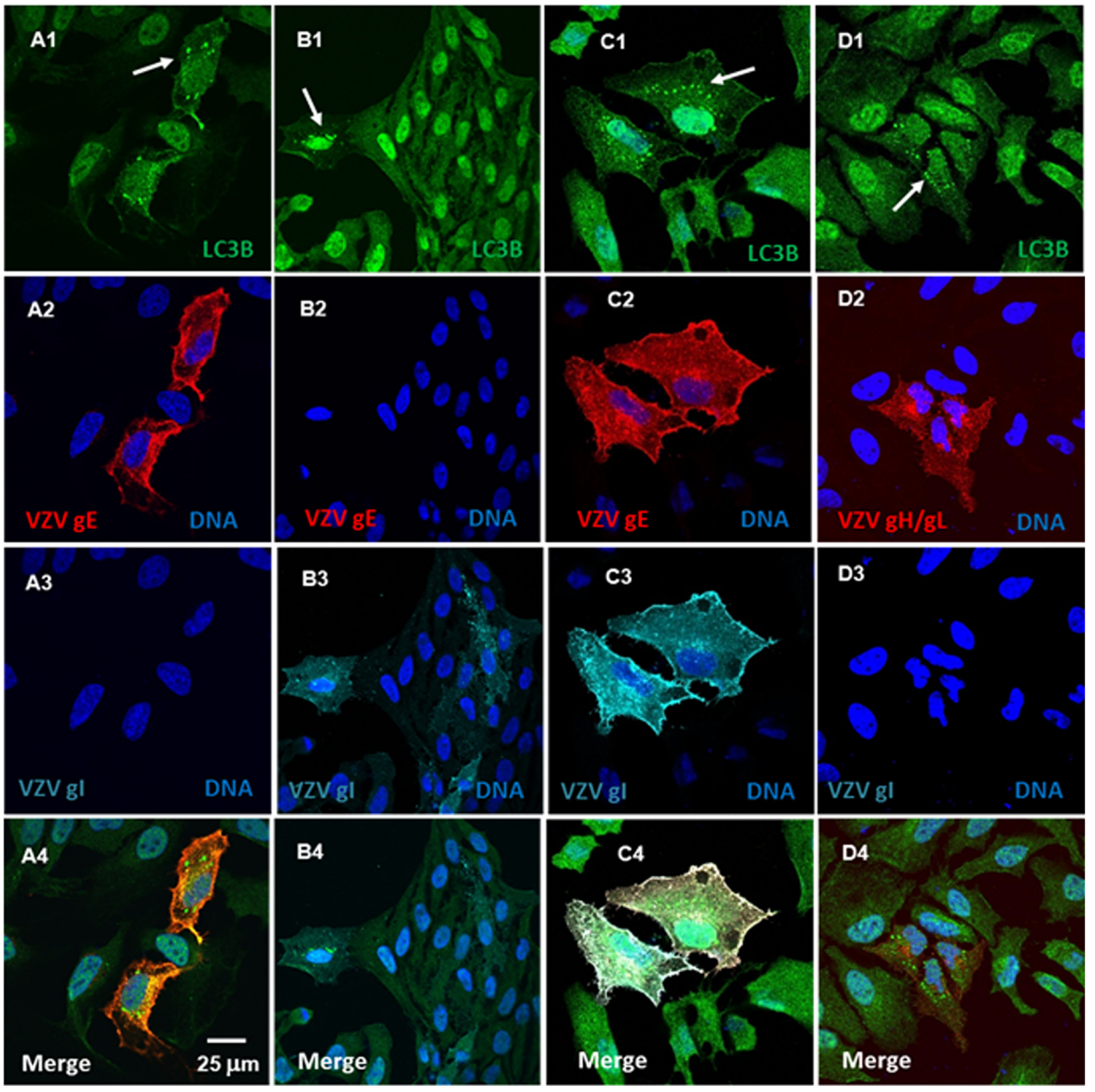

FIG. 6. Expression of VZV glycoproteins was sufficient to induce increased autophagy in transfected cells. HeLa cells were plated onto coverslips in a six-well plate and grown to 50% confluence before transfection with PTargeT VZV gE, gI, gH, and gL plasmid constructs (0.5 μg/ml of DNA per construct), either singly or in combinations of gE/gI and gH/gL. The medium was replaced at 6 h posttransfection, and the cells were incubated at 37°C for periods up to 24 h. The cells were then fixed, permeabilized, and labeled with antibodies to LC3B and the VZV glycoproteins (Table 1), together with the Hoechst 33342 nuclear stain (blue). The coverslips were inverted onto slides and viewed in a fluorescence confocal microscope. (A1 to A4) Transfection with VZV gE alone. (B1 to B4) Transfection with VZV gI alone. (C1 to C4) Transfection with VZV gE/gI complex). (D1 to D4) Transfection with VZV gH/gL complex. (A1 to A4) Two cells expressed VZV gE (red); both showed increased punctate LC3B (green) staining (white arrow) characteristic of autophagosomes. (B1 to B4) Five cells expressed VZV gI (cyan), with one showing increased punctate LC3B staining (white arrow). (C1 to C4) Two cells coexpressed both VZV gE (red) and VZV gI (cyan); both cells showed increased punctate LC3B (green) staining (white arrow). (D1 to D4) Three cells expressed both VZV gH (red) and VZV gL (unlabeled); all exhibited punctate LC3B (green) staining (white arrow). There were cells in each panel that did not express either VZV glycoprotein and did not show increased punctate LC3B (green) immunoreactivity.

this difference was related to a higher growth rate of HeLa cells than of MRC-5 fibroblasts. Transfected HeLa cells strongly expressing VZV gE exhibited ER-to-nuclear area ratios ranging up to 3, i.e., the ER was three times the size of the nucleus or three times larger than the ER in nontransfected HeLa cells. Cells that only weakly expressed VZV gE did not exhibit a greatly expanded ER size. Similarly high ER ratios were observed in transfected cells expressing large amounts of gI individually or both gE and gI together (data not shown).

Alternative splicing of XBP1 and upregulation of CHOP: markers unique to the unfolded protein response during VZV infection. To further document that the UPR to ER stress is

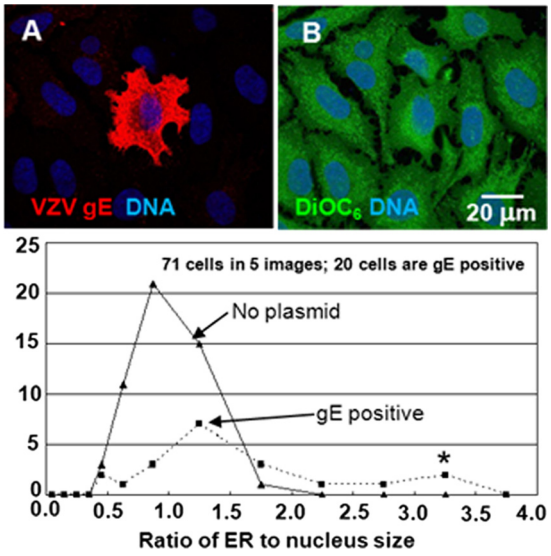

FIG. 7. Transient transfection of VZV gE induced a larger ER in cells expressing the glycoprotein. HeLa cells were plated onto coverslips in a six-well plate and subsequently transfected with the PTargeT gE plasmid construct (0.5 μg/ml of DNA), as previously described. For the final 30 min of incubation, the cells were stained with the polar dye $DiOC_6$. The cells were then fixed, permeabilized, and labeled with antibodies to VZV gE, together with the Hoechst 33342 nuclear stain. The coverslips were inverted onto slides and viewed in a fluorescence confocal microscope. (A) Among several cells (nuclei, blue) was a single transfected cell with a bright red (gE) cytoplasmic staining pattern. (B) Note the $DiOC_6$ staining of the same cluster of cells, with the intense $DiOC_6$ labeling of the ER in the VZV gE-positive cell. (Graph) Nuclear and ER sizes were measured in 5 images containing 71 cells (20 expressing VZV gE), and the corresponding ratio was calculated and plotted. Cells not expressing the viral glycoprotein exhibited an ER about the same size as the nucleus, whereas cells expressing VZV gE exhibited an expanded ER, with a range from slightly larger to 3-fold larger. The cells that exhibited the largest ER typically exhibited more intense glycoprotein expression. For example, the ratio for the bright gE-positive cell in panel A is indicated by the asterisk.

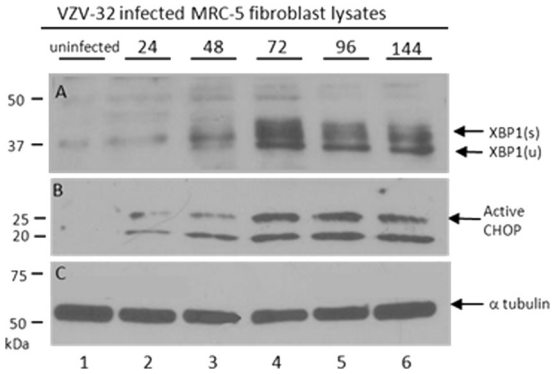

FIG. 8. VZV infection led to alternative splicing of UPR transcription factor XBP1 as well as upregulation of CHOP. MRC-5 cells were grown to confluence in 25-cm monolayers and then inoculated with VZV-infected cells. Individual monolayers were lysed at 0, 24, 48, 72, 96, and 144 hpi; solubilized; subjected to SDS-PAGE; transferred to a PVDF membrane; and immunoblotted with rabbit polyclonal antibodies to XBP1 and CHOP separately. (A) From 48 to 144 hpi (lanes 3 to 6), closely migrating bands appeared at 40 to 45 kDa that corresponded to the spliced form of XBP1 (s). Similarly, the band corresponding to unspliced XBP1 appeared more prominent later in the infection (u). (B) Active CHOP at 29 kDa was upregulated in concert with the alternatively spliced form of XBP1. (C) Bands corresponding to α-tubulin were similar in all lanes and served as a loading control for the Western blots.

occurring in VZV-infected cells, we probed for XBP1 and CHOP proteins at timed intervals during the VZV infectious cycle in cultured cells. As part of the UPR, XBP1 mRNA is upregulated by the ER sensor protein ATF6 and alternatively spliced by another ER sensor protein, IRE1 (3, 57). The alternative splicing of the XBP1 mRNA results in a frameshift in the C terminus of the translated protein that exposes a basic leucine zipper (bZIP) transcription factor; the spliced XBP1 variant contains 115 more amino acids than the unspliced form, which is 261 residues in length. We found that the bands for the alternatively spliced higher-molecular-weight form, XBP1(s), first became detectable at 48 hours postinfection (hpi) and were readily visible at both 72 and 96 hpi (Fig. 8). These results demonstrated unequivocally that the IRE1 arm of the UPR was upregulated in VZV-infected cells—another distinctive sign of a VZV-induced ER stress response.

One of the proteins induced by XBP1 and ATF4 (another UPR component) under conditions of severe ER stress is CHOP or GADD153 (growth arrest and DNA damage 153). CHOP is a 29-kDa protein that is a member of the C/EBP family of transcription factors; CHOP production has been primarily associated with persistent ER stress and subsequent stress-mediated apoptosis (35). But it also appears to play roles in mediating oxidative stress in mitochondria (40). In VZV-infected monolayers incubated for 48 h, CHOP was upregulated in concert with the appearance of the spliced form of XBP1 (Fig. 8B). These dual concordant results suggested that as most of the cells became infected, the conditions of ER stress in the cells became extreme.

DISCUSSION

Autophagosomes were easily and abundantly detected in a variety of vesicle samples from human cases of varicella and zoster. Thus, we have greatly extended earlier findings in which we detected autophagosomes in a biopsy sample from one case of human zoster (47). In other words, we have demonstrated that autophagy occurs during both primary VZV infection and VZV reactivation within the skin vesicle, the final site of virion assembly and envelopment. In turn, these results strongly suggest that autophagy is a previously unrecognized component of VZV pathogenesis. The prominence of autophagosome formation was all the more unpredictable, because the VZV genome lacks the HSV γ34.5 gene, which product can inhibit autophagy and thereby enhance viral virulence. A reasonable hypothesis, based on the HSV data with ICP34.5 null virus (30), would have proposed that autophagy unfettered by ICP34.5 would eliminate all VZV and that disease would be minimal. The fact that VZV causes disease leads us to propose in the paragraphs below that autophagy serves a role in VZV infection entirely different from that proposed for HSV infection.

Analyses of VZV vesicle cells were important also to demonstrate that autophagy in VZV-infected cells represented an authentic environment within the human with VZV disease. In

that regard, we discovered that the percentage of infected vesicular keratinocytes that contained autophagosomes was equal to or higher than that observed in VZV-infected cultured cells (>70% versus <20%). This difference is possibly due to well-known low VZV titers of virus grown in cultured cells; thus, the titer of inoculum virus is invariably low (6). Further, the findings in vesicular keratinocytes confirmed an unexpected earlier result in VZV-infected cultured cells, namely, that autophagosome formation was detectable before VZV entered the late kinetic phase of replication. In contrast, autophagy associated with other viruses is often thought to be a relatively late event in the virus life cycle (29). When taken together, these data suggest that autophagy may be a proviral event in that autophagy would prolong the life of a cell infected with VZV and thereby diminish apoptosis. This property would be more important for a cell-associated alphaherpesvirus, such as VZV, while less critical for the more lytic HSV-1 counterpart.

The data with tunicamycin treatment were of particular interest to our laboratory because we had used tunicamycin frequently in past experiments to determine the nonglycosylated precursor forms for the VZV glycoproteins (32). Tunicamycin is extremely effective because the chemical blocks the enzyme GlcNAc phosphotransferase, which catalyzes the transfer of *N*-acetylglucosamine-1-phosphate from UDP-*N*-acetylglucosamine to dolichol phosphate, the essential first step of glycoprotein biosynthesis in the ER (51). Thus, misfolded precursor glycoprotein forms accumulate quickly in the ER, a process now known to lead to ER stress and subsequent autophagosome accumulation. In fact, tunicamycin-treated uninfected cells are a common positive control for induction of autophagy under any other experimental condition (27). We availed ourselves of this experimental model to show the remarkable similarity of autophagy in VZV-infected cells to autophagy in tunicamycin-treated but uninfected cells. We also repeated the tunicamycin experiment in infected cells and showed no noticeable increase in autophagosome formation. In other words, VZV infection by itself was a very effective inducer of autophagy in cultured cells.

ER stress is well recognized as one precursor to autophagy through the induction of the UPR (42). During an earlier analysis of chromatographically purified VZV glycoprotein gE by Orbitrap mass spectrometry, we had identified four proteins associated with the UPR (including 3 heat shock proteins, HSPA5, HSPA8, and HSPD1) copurifying with gE (8). Together with the tunicamycin data, these latter results strongly supported a role for glycoproteins in the pathway of ER stress and UPR leading to autophagy in VZV-infected cells. These results were further strengthened by our current data with transient transfections expressing VZV glycoproteins gE/gI and gH/gL. ER stress was quickly documented by increased ER size, and autophagy was demonstrated by the appearance of punctate autophagosomes within 24 h posttransfection.

One observation in this work is that the response of any given cell to a stress such as tunicamycin treatment, transient transfection of VZV glycoprotein genes, or even VZV infection is variable. For example, we documented that 30% of the cells treated with tunicamycin exhibited increased LC3B puncta typical of increased autophagosomes. While 30% is significantly more than the basal rate in untreated cells, we questioned why all of the cells which experienced the same stress did not exhibit the same response (increased autophagosomes). The answer is likely that the response of the cell to stress, such as tunicamycin treatment, may be affected by the cell cycle status of the cell. For example, a cell in a resting G_0 state may not respond as quickly or as extensively as a cell in a more active metabolic state such as those associated with an actively dividing cell (e.g., G_1 or G_2).

As mentioned above, any condition that creates an imbalance between glycoprotein biosynthesis and the protein-folding capacity of the ER leads to ER stress, which is relieved by the UPR. In turn, the UPR activates three linked signal transduction pathways via three ER stress sensors: (i) IRE1 (inositol-requiring enzyme 1), (ii) PERK (PKR-like eIF2a kinase), and (iii) ATF6 (activating transcription factor 6). When the IRE1 pathway is activated, the endoribonuclease IRE1 executes site-specific cleavage of XBP1 mRNA to produce a spliced transcript that codes for a potent 45-kDa bZIP transcriptional activator of the UPR, called XBP1s protein. We were able to detect the XBP1s protein in VZV-infected cells by immunoblotting, further proof that ER stress had activated the UPR following VZV infection of cultured cells. To provide additional evidence for VZV-induced stress, we successfully probed for a second transcription factor called CHOP, which is closely associated with activation of the PERK UPR pathway (39). In a similar experiment performed with antibody reagents from the same commercial source, the CHOP protein has recently been detected in cells under stress after infection with mycobacteria (44). When taken together, our data suggest that autophagy may be a proviral event in that the UPR moderates the level of ER stress in infected cells and thus prolongs the life of an infected cell. In a recent report about murine gammaherpesvirus 68, investigators similarly proposed that herpesvirus 68 can manipulate the autophagy machinery in order to promote the survival of infected endothelial cells (46).

These postulated proviral effects differ remarkably from the ascribed roles of autophagy during infection with another closely related human alphaherpesvirus, namely, HSV-1. The HSV γ34.5 neurovirulence gene interacts with Beclin 1 (Atg6 yeast homolog), an essential autophagy protein and component of a complex containing the enzymatic and regulatory subunits of class III phosphatidylinositol 3-kinase (Vps34 and Vps15) (1, 34). For example, recent HSV experiments suggest that the interaction of HSV ICP34.5 with Beclin 1 diminishes autophagy-mediated MHC class II antigen presentation and thereby enhances HSV-1 neuropathogenesis in an animal model (30). Since VZV has evolved as the human herpesvirus with the smallest genome, lacking any ICP34.5 ortholog, VZV presumably has yielded its ability to circumvent the cellular autophagy pathways during its life cycle.

ACKNOWLEDGMENTS

We thank the University of Iowa Central Microscopy Research Facility for their assistance.

This research was supported by NIH grant AI89716 (C.G.) as well as funding from Merck, Sharp & Dohme.

REFERENCES

1. **Abeliovich, H., W. A. Dunn, Jr., J. Kim, and D. J. Klionsky.** 2000. Dissection of autophagosome biogenesis into distinct nucleation and expansion steps. J. Cell Biol. **151:**1025–1034.

2. **Arvin, A. M., et al.** 2010. Varicella-zoster virus T cell tropism and the pathogenesis of skin infection. Curr. Top. Microbiol. Immunol. **342:**189–209.
3. **Back, S. H., M. Schroder, K. Lee, K. Zhang, and R. J. Kaufman.** 2005. ER stress signaling by regulated splicing: IRE1/HAC1/XBP1. Methods **35:**395–416.
4. **Brunner, S., et al.** 2000. Cell cycle dependence of gene transfer by lipoplex, polyplex and recombinant adenovirus. Gene Ther. **7:**401–407.
5. **Buchkovich, N. J., T. G. Maguire, A. W. Paton, J. C. Paton, and J. C. Alwine.** 2009. The endoplasmic reticulum chaperone BiP/GRP78 is important in the structure and function of the HCMV assembly compartment. J. Virol. **83:** 11421–11428.
6. **Carpenter, J. E., E. P. Henderson, and C. Grose.** 2009. Enumeration of an extremely high particle-to-PFU ratio for varicella-zoster virus. J. Virol. **83:** 6917–6921.
7. **Carpenter, J. E., J. A. Hutchinson, W. Jackson, and C. Grose.** 2008. Egress of light particles among filopodia on the surface of varicella-zoster virus-infected cells. J. Virol. **82:**2821–2835.
8. **Carpenter, J. E., W. Jackson, G. A. deSouza, L. Haarr, and C. Grose.** 2010. Insulin degrading enzyme binds to the nonglycosylated precursor of varicella-zoster virus gE protein found in the endoplasmic reticulum. J. Virol. **84:**847–855.
9. **Davison, A. J.** 1991. Varicella-zoster virus. The fourteenth Fleming lecture. J. Gen. Virol. **72:**475–486.
10. **Davison, A. J., and J. E. Scott.** 1986. The complete DNA sequence of varicella-zoster virus. J. Gen. Virol. **67:**1759–1816.
11. **Dengjel, J., et al.** 2005. Autophagy promotes MHC class II presentation of peptides from intracellular source proteins. Proc. Natl. Acad. Sci. U. S. A. **102:**7922–7927.
12. **Deretic, V., and B. Levine.** 2009. Autophagy, immunity, and microbial adaptations. Cell Host Microbe **5:**527–549.
13. **Dorner, A. J., L. C. Wasley, and R. J. Kaufman.** 1989. Increased synthesis of secreted proteins induces expression of glucose-regulated proteins in butyrate-treated Chinese hamster ovary cells. J. Biol. Chem. **264:**20602–20607.
14. **Dreux, M., and F. V. Chisari.** 2009. Autophagy proteins promote hepatitis C virus replication. Autophagy **5:**1224–1225.
15. **Dreux, M., P. Gastaminza, S. F. Wieland, and F. V. Chisari.** 2009. The autophagy machinery is required to initiate hepatitis C virus replication. Proc. Natl. Acad. Sci. U. S. A. **106:**14046–14051.
16. **Duus, K. M., C. Hatfield, and C. Grose.** 1995. Cell surface expression and fusion by the varicella-zoster virus gH:gL glycoprotein complex: analysis by laser scanning confocal microscopy. Virology **210:**429–440.
17. **Eisfeld, A. J., S. E. Turse, S. A. Jackson, E. C. Lerner, and P. R. Kinchington.** 2006. Phosphorylation of the varicella-zoster virus (VZV) major transcriptional regulatory protein IE62 by the VZV open reading frame 66 protein kinase. J. Virol. **80:**1710–1723.
18. **English, L., et al.** 2009. Autophagy enhances the presentation of endogenous viral antigens on MHC class I molecules during HSV-1 infection. Nat. Immunol. **10:**480–487.
19. **Espert, L., P. Codogno, and M. Biard-Piechaczyk.** 2007. Involvement of autophagy in viral infections: antiviral function and subversion by viruses. J. Mol. Med. **85:**811–823.
20. **Grose, C.** 1990. Glycoproteins encoded by varicella-zoster virus: biosynthesis, phosphorylation, and intracellular trafficking. Annu. Rev. Microbiol. **44:**59–80.
21. **Grose, C., and P. A. Brunel.** 1978. Varicella-zoster virus: isolation and propagation in human melanoma cells at 36 and 32 degrees C. Infect. Immun. **19:**199–203.
22. **Grose, C., S. Vleck, O. A. Karlsen, and E. A. Montalvo.** 2011. Structure-function profiles of nine varicella-zoster virus glycoproteins: endocytosis, entry and egress, p. 153–174. *In* S. K. Weller (ed.), Alphaherpesviruses: molecular virology. Caister Academic Press, Norwich, Norfolk, United Kingdom.
23. **Hotchkiss, R. S., A. Strasser, J. E. McDunn, and P. E. Swanson.** 2009. Cell death. N. Engl. J. Med. **361:**1570–1583.
24. **Isler, J. A., A. H. Skalet, and J. C. Alwine.** 2005. Human cytomegalovirus infection activates and regulates the unfolded protein response. J. Virol. **79:**6890–6899.
25. **Jacobsen, L. B., S. A. Calvin, K. E. Colvin, and M. Wright.** 2004. FuGENE 6 transfection reagent: the gentle power. Methods **33:**104–112.
26. **Kabeya, Y., et al.** 2000. LC3, a mammalian homologue of yeast Apg8p, is localized in autophagosome membranes after processing. EMBO J. **19:**5720–5728.
27. **Klionsky, D. J., et al.** 2008. Guidelines for the use and interpretation of assays for monitoring autophagy in higher eukaryotes. Autophagy **4:**151–175.
28. **Ku, C. C., J. Besser, A. Abendroth, C. Grose, and A. M. Arvin.** 2005. Varicella-zoster virus pathogenesis and immunobiology: new concepts emerging from investigations with the SCIDhu mouse model. J. Virol. **79:** 2651–2658.
29. **Kudchodkar, S. B., and B. Levine.** 2009. Viruses and autophagy. Rev. Med. Virol. **19:**359–378.
30. **Leib, D. A., D. E. Alexander, D. Cox, J. Yin, and T. A. Ferguson.** 2009. Interaction of ICP34.5 with Beclin 1 modulates herpes simplex virus type 1 pathogenesis through control of CD4+ T-cell responses. J. Virol. **83:**12164–12171.
31. **Lin, L. T., P. W. Dawson, and C. D. Richardson.** 2010. Viral interactions with macroautophagy: a double-edged sword. Virology **402:**1–10.
32. **Montalvo, E. A., R. T. Parmley, and C. Grose.** 1985. Structural analysis of the varicella-zoster virus gp98-gp62 complex: posttranslational addition of N-linked and O-linked oligosaccharide moieties. J. Virol. **53:**761–770.
33. **Nakatsukasa, K., and J. L. Brodsky.** 2008. The recognition and retrotranslocation of misfolded proteins from the endoplasmic reticulum. Traffic **9:**861–870.
34. **Orvedahl, A., et al.** 2007. HSV-1 ICP34.5 confers neurovirulence by targeting the Beclin 1 autophagy protein. Cell Host Microbe **1:**23–35.
35. **Oyadomari, S., and M. Mori.** 2004. Roles of CHOP/GADD153 in endoplasmic reticulum stress. Cell Death Differ. **11:**381–389.
36. **Perera, L. P., J. D. Mosca, W. T. Ruyechan, and J. Hay.** 1992. Regulation of varicella-zoster virus gene expression in human T lymphocytes. J. Virol. **66:**5298–5304.
37. **Peters, G. A., et al.** 2006. A full-genome phylogenetic analysis of varicella-zoster virus reveals a novel origin of replication-based genotyping scheme and evidence of recombination between major circulating clades. J. Virol. **80:**9850–9860.
38. **Pohl, C.** 2009. Dual control of cytokinesis by the ubiquitin and autophagy pathways. Autophagy **5:**561–562.
39. **Raven, J. F., and A. E. Koromilas.** 2008. PERK and PKR: old kinases learn new tricks. Cell Cycle **7:**1146–1150.
40. **Rutkowski, D. T., and R. S. Hegde.** 2010. Regulation of basal cellular physiology by the homeostatic unfolded protein response. J. Cell Biol. **189:**783–794.
41. **Sabnis, R. W., T. G. Deligeorgiev, M. N. Jachak, and T. S. Dalvi.** 1997. DiOC6(3): a useful dye for staining the endoplasmic reticulum. Biotech. Histochem. **72:**253–258.
42. **Schroder, M.** 2008. Endoplasmic reticulum stress responses. Cell. Mol. Life Sci. **65:**862–894.
43. **Schroder, M., and R. J. Kaufman.** 2005. The mammalian unfolded protein response. Annu. Rev. Biochem. **74:**739–789.
44. **Seimon, T. A., et al.** 2010. Induction of ER stress in macrophages of tuberculosis granulomas. PLoS One **5:**e12772.
45. **Shoji-Kawata, S., and B. Levine.** 2009. Autophagy, antiviral immunity, and viral countermeasures. Biochim. Biophys. Acta **1793:**1478–1484.
46. **Suarez, A. L., et al.** 2011. Gammaherpesvirus 68 infection of endothelial cells requires both host autophagy genes and viral oncogenes for optimal survival and persistence. J. Virol. **85:**6293–6308.
47. **Takahashi, M. N., et al.** 2009. Varicella-zoster virus infection induces autophagy in both cultured cells and human skin vesicles. J. Virol. **83:**5466–5476.
48. **Tanida, I.** 2011. Autophagosome formation and molecular mechanism of autophagy. Antioxid. Redox Signal. **14:**2201–2214.
49. **Tanida, I., T. Ueno, and E. Kominami.** 2004. LC3 conjugation system in mammalian autophagy. Int. J. Biochem. Cell Biol. **36:**2503–2518.
50. **Terasaki, M., and T. S. Reese.** 1992. Characterization of endoplasmic reticulum by co-localization of BiP and dicarbocyanine dyes. J. Cell Sci. **101:**315–322.
51. **Tkacz, J. S., and O. Lampen.** 1975. Tunicamycin inhibition of polyisoprenyl N-acetylglucosaminyl pyrophosphate formation in calf-liver microsomes. Biochem. Biophys. Res. Commun. **65:**248–257.
52. **Tournier, P., F. Cathala, and W. Bernhard.** 1957. Ultrastructure and intracellular development of varicella virus observed with electron microscope. Presse Med. **65:**1229–1234.
53. **Tranchant, I., B. Thompson, C. Nicolazzi, N. Mignet, and D. Scherman.** 2004. Physicochemical optimisation of plasmid delivery by cationic lipids. J. Gene Med. **6**(Suppl. 1)**:**S24–S35.
54. **Weigle, K. A., and C. Grose.** 1983. Common expression of varicella-zoster viral glycoprotein antigens in vitro and in chickenpox and zoster vesicles. J. Infect. Dis. **148:**630–638.
55. **Weller, T. H.** 1983. Varicella and herpes zoster. Changing concepts of the natural history, control, and importance of a not-so-benign virus. N. Engl. J. Med. **309:**1434–1440.
56. **Yang, Z., and D. J. Klionsky.** 2009. An overview of the molecular mechanism of autophagy. Curr. Top. Microbiol. Immunol. **335:**1–32.
57. **Yoshida, H., T. Matsui, A. Yamamoto, T. Okada, and K. Mori.** 2001. XBP1 mRNA is induced by ATF6 and spliced by IRE1 in response to ER stress to produce a highly active transcription factor. Cell **107:**881–891.